electronics

MDPI

Communication

Real-Time-Sensing-Assisted Intelligent Communication for Internet of Things

Shengfeng Zhang [1,2], Lizhi Qin [3,*] and Weixing Sheng [2]

[1] The 8th Research Academy of China State Shipbuilding Corporation, Nanjing 211153, China; zhang_shengfeng@126.com
[2] School of Electronic and Optical Engineering, Nanjing University of Science and Technology, Nanjing 210094, China; shengwx@njust.edu.cn
[3] National Key Laboratory of Wireless Communications, University of Electronic Science and Technology of China, Chengdu 611731, China
* Correspondence: 202312220625@std.uestc.edu.cn

Abstract

With the rapid development of the Internet of Things (IoT), electromagnetic devices are increasingly being deployed in dense and resource-limited environments, resulting in severe mutual interference within limited spectral and spatial resources. To address this issue, a real-time sensing-assisted intelligent communication method is proposed which adaptively selects appropriate communication schemes based on the electromagnetic environment to achieve robust, intelligent communication. A key challenge lies in mitigating the self-interference caused by the communication transmit signal on wideband sensing. Focusing on self-interference suppression for wideband sensing receivers, this paper first presents a self-interference reconstruction and suppression architecture. Then, a closed-form expression for suppression performance is theoretically derived, and the impact of imperfect time synchronization between the interference and reference signals on suppression effectiveness is analyzed. Simulation results verify the theoretical analysis and demonstrate that, under identical normalized fractional delays, the degradation in interference suppression performance of the compressed sensing-based receiver is smaller than that of the uncompressed receiver. Specifically, when the normalized time synchronization error is 0.5, the 2-fold compressed wideband receiver achieves a 6.9 dB improvement in suppression capability compared to the uncompressed receiver.

Keywords: self-interference; compressive sensing; interference suppression; Nyquist folding; full duplex

check for updates

Academic Editor: Paulo Pereira Monteiro

Received: 18 August 2025
Revised: 10 September 2025
Accepted: 18 September 2025
Published: 18 September 2025

Citation: Zhang, S.; Qin, L.; Sheng, W. Real-Time-Sensing-Assisted Intelligent Communication for Internet of Things. *Electronics* **2025**, *14*, 3707. https://doi.org/10.3390/electronics14183707

Copyright: © 2025 by the authors. Licensee MDPI, Basel, Switzerland. This article is an open access article distributed under the terms and conditions of the Creative Commons Attribution (CC BY) license (https://creativecommons.org/licenses/by/4.0/).

1. Introduction

With the rapid growth of the Internet of Things (IoT), electromagnetic devices are increasingly deployed in dense and resource-limited environments [1]. For example, in smart homes, various wireless technologies such as 4G, 5G, Wi-Fi, Bluetooth, NearLink, and LoRa operate concurrently within a confined space. This co-existence leads to severe mutual interference due to limited spectral and spatial resources [2].

To alleviate such interference, sensing-assisted communication has emerged as a promising solution. In traditional designs, spectrum sensing and data transmission are often separated in time, making it difficult to capture rapidly changing interference conditions [3]. Real-time sensing-assisted communication has been proposed to address this issue by enabling concurrent sensing and transmission [4]. This allows the system to continuously

monitor environmental interference and dynamically adjust transmission parameters to maintain reliable communication [5].

In this context, the Nyquist Folding Receiver (NYFR) offers an efficient front-end architecture for real-time wideband sensing. Developed by Fudge et al. based on compressed sensing (CS) theory [6], the NYFR acquires digitally sparse or compressible wideband signals at sub-Nyquist rates. These signals can be directly processed in the time-frequency domain or reconstructed using CS algorithms [7]. Existing NYFR research mainly focuses on feature extraction, modulation classification [8], signal detection, and parameter estimation from compressed signals [9].

A key challenge in implementing real-time sensing-assisted communication is the severe self-interference induced by the high-power transmit signal on the NYFR front-end [10]. Without effective suppression, the sensing performance degrades significantly, making it difficult to respond to rapidly varying interference in real time.

Self-interference suppression methods generally fall into three categories: spatial domain, radio frequency (RF) domain, and digital domain suppression [11]. Spatial domain methods improve antenna isolation [12], RF domain suppression cancels interference by adjusting the amplitude, phase, and delay of reference signals using analog circuitry [13], and digital domain suppression estimates and reconstructs the interference signal in the baseband domain [14]. However, all these methods are sensitive to hardware imperfections and algorithmic constraints [15], such as time synchronization errors [16] and sampling clock offset [17]. Furthermore, most existing work focuses on conventional receivers, with limited studies addressing self-interference suppression in wideband compressive receivers like the NYFR.

To bridge this gap, this paper studies digital domain self-interference suppression, addressing a key challenge in real-time sensing-assisted intelligent communication. A suppression architecture based on the NYFR is proposed, where compressed signals are utilized to estimate and cancel self-interference. A closed-form expression quantifying suppression performance is derived, and the theoretical impact of fractional delay on suppression effectiveness is analyzed. Both analytical and simulation results demonstrate that, under identical timing errors, the CS-based receiver outperforms its uncompressed counterpart in interference suppression.

The main contributions of this paper are as follows:

- A self-interference suppression architecture based on the NYFR is proposed, enabling real-time wideband spectrum sensing and communication at sub-Nyquist rates.
- A theoretical model is developed to quantify the effect of time synchronization errors on suppression performance in the compressed domain, with a closed-form expression derived under fractional delay.
- Simulations validate the theoretical analysis, showing that under a normalized delay of 0.5, the 2-fold compressed receiver achieves 6.9 dB better suppression than the uncompressed receiver.

2. System Model

In dense IoT environments, various wireless devices operate simultaneously, causing severe mutual interference. As illustrated in Figure 1, to enable reliable wideband spectrum sensing, the electronic transmitter's self-interference signal is directly fed to the wideband sensing receiver via a wired connection, serving as a reference for suppression. The receiver adopts the Nyquist Folding Receiver (NYFR) architecture as its front-end, and digital domain self-interference suppression is performed on the compressed signals to extract the desired signals from the interference-laden environment.

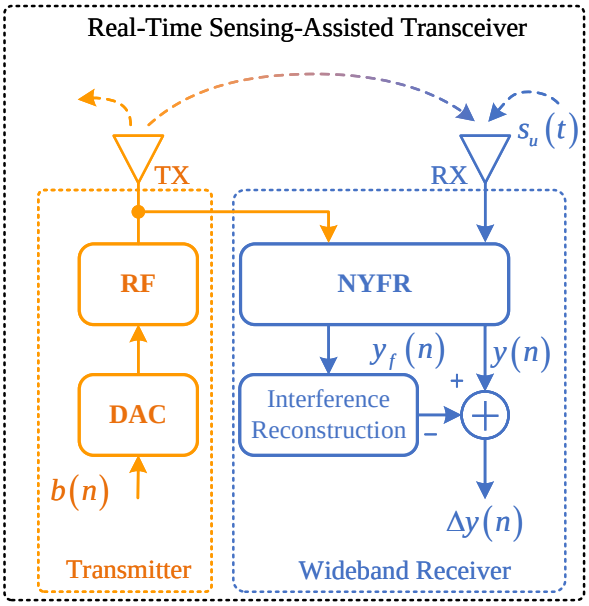


Figure 1. System model of real-time sensing-assisted transceivers.

2.1. Transmitter

The baseband signal of the transmitter is denoted as $b(n)$. After passing through the digital-to-analog converter (DAC), it becomes the continuous time signal $b(t)$, which is then upconverted to the RF signal $s_i(t)$

$$s_i(t) = b(t)e^{j(2\pi f_i t + \varphi_i(t))}, \tag{1}$$

where f_i is the carrier frequency, and $\varphi_i(t)$ represents the initial phase.

2.2. Channel

Assuming a flat fading channel, the self-interference signal $r_i(t)$ received at the wideband receiver is modeled as

$$r_i(t) = H_i s_i(t - \tau), \tag{2}$$

where H_i denotes the self-interference channel attenuation factor, and τ is the relative delay between the self-interference and the reference signal.

The overall received signal $r(t)$ at the wideband receiver can be expressed as

$$r(t) = r_i(t) + r_u(t) + v(t), \tag{3}$$

where $r_i(t)$ denotes the self-interference, $r_u(t)$ is the desired signal of interest (SOI), and $v(t)$ represents the effective noise term. Here, the noise term not only includes additive white Gaussian noise (AWGN), but also accounts for RF imperfections such as Power Amplifier (PA) nonlinearity and I/Q imbalance, as well as various colored noise components. When a sufficient number of independent noise sources are present, by the Central Limit Theorem, the composite noise can be reasonably approximated as a complex Gaussian distribution.

The transmitted self-interference signal $s_i(t)$ is also coupled to the receiver through a wired connection, serving as the reference signal $r_f(t)$ for digital self-interference reconstruction and cancellation:

$$r_f(t) = s_i(t). \tag{4}$$

2.3. Wideband Receiver

After down-conversion and analog-to-digital conversion (ADC), the self-interference signal $r_i(n)$, the received signal $r(n)$, and the reference signal $r_f(n)$ are expressed as

$$r_i(n) = H_i s_i(n-\tau), \tag{5}$$
$$r(n) = r_i(n) + r_u(n) + v(n), \tag{6}$$
$$r_f(n) = s_i(n). \tag{7}$$

The delay τ can be decomposed as $\tau = D + \Delta D$, where D is the integer multiple of the sampling period delay between the self-interference and the reference signals, which can be accurately estimated and compensated by existing time synchronization algorithms [18]. ΔD denotes the residual fractional delay, satisfying $0 \leq |\Delta D| \leq 0.5$. This paper focuses on the impact of the fractional delay ΔD on self-interference suppression performance, i.e., we consider $\tau = \Delta D$.

After synchronization, the signals are represented as

$$r_i(n) = H_i b(n-\Delta D), \tag{8}$$
$$r(n) = r_i(n) + r_u(n) + v_0(n) = H_i b(n-\Delta D) + r_u(n) + v_0(n), \tag{9}$$
$$r_f(n) = b(n), \tag{10}$$

where $b(n)$ denotes the baseband self-interference signal.

For vector representation with length N, the signals can be written as

$$\mathbf{r}_i = [r_i(n+1), r_i(n+2), \ldots, r_i(n+N)]^T, \tag{11}$$
$$\mathbf{r} = [r(n+1), r(n+2), \ldots, r(n+N)]^T, \tag{12}$$
$$\mathbf{r}_f = [r_f(n+1), r_f(n+2), \ldots, r_f(n+N)]^T. \tag{13}$$

3. CS-Based Wideband Receiver

This section presents the self-interference suppression framework based on a CS wideband receiver. The signal processing flow consists of three main modules: NYFR, self-interference suppression, and reconstruction of the SOI.

3.1. NYFR-Based Signal Folding

The NYFR enables sub-Nyquist sampling for spectrally sparse signals. If the input signal $\mathbf{r}$ is sparse or compressible in some domain [19], it can be compressed as

$$\mathbf{y} = \boldsymbol{\varphi}\mathbf{r}, \tag{14}$$

where $\boldsymbol{\varphi}$ denotes the measurement matrix with dimension $M \times N$, $M \ll N$.

The measurement matrix $\boldsymbol{\varphi}$ can be expressed in terms of its row selection index vector $\boldsymbol{\alpha} = [\alpha_1, \alpha_2, \ldots, \alpha_M]$ as

$$\boldsymbol{\varphi} = \begin{bmatrix} \varphi_{1,1} & \cdots & \varphi_{1,N} \\ \vdots & \ddots & \vdots \\ \varphi_{M,1} & \cdots & \varphi_{M,N} \end{bmatrix}, \tag{15}$$

where $\varphi_{k,\alpha_k} = 1$ and all other elements are zero.

By substituting Equations (11)–(13) into (14), we obtain the compressed self-interference signal $\mathbf{y}_i$, the received signal $\mathbf{y}$, and the reference signal $\mathbf{y}_f$ as

$$\mathbf{y}_i = \boldsymbol{\varphi}\mathbf{r}_i = H_i[b(n+\alpha_1-\Delta D),\ldots,b(n+\alpha_M-\Delta D)]^T, \tag{16}$$

$$\begin{aligned}\mathbf{y} &= \boldsymbol{\varphi}\mathbf{r} = \boldsymbol{\varphi}(\mathbf{r}_i+\mathbf{r}_u+\mathbf{v})\\ &= H_i[b(n+\alpha_1-\Delta D),\ldots,b(n+\alpha_M-\Delta D)]^T+\mathbf{y}_u+\mathbf{v}_\varphi,\end{aligned} \tag{17}$$

$$\mathbf{y}_f = \boldsymbol{\varphi}\mathbf{r}_f = [b(n+\alpha_1),\ldots,b(n+\alpha_M)]^T. \tag{18}$$

Here, $\mathbf{r}_u$ and $\mathbf{y}_u = \boldsymbol{\varphi}\mathbf{r}_u$ denote the SOI before and after compression, while $\mathbf{v}$ and $\boldsymbol{v}_\varphi = \boldsymbol{\varphi}\boldsymbol{v}$ represent the additive white Gaussian noise (AWGN) before and after compression, respectively.

3.2. Self-Interference Suppression

To mitigate the self-interference resulting from the concurrent transmission and reception on integrated jamming and sensing platforms, a digital domain self-interference suppression method is applied. Based on the compressed reference signal, self-interference reconstruction and cancellation are performed by subtracting the reconstructed interference from the compressed received signal.

As illustrated in Figure 2, an L-order linear filter is used to reconstruct the compressed self-interference signal as

$$y'_f(n+\alpha_k) = \sum_{l=1}^{L}\omega_l(n+\alpha_k)y_f(n+\alpha_{k-l+1}), \tag{19}$$

where $\omega_l(n+\alpha_k)$ denotes the tap coefficient of the l-th filter at time index $n+\alpha_k$.

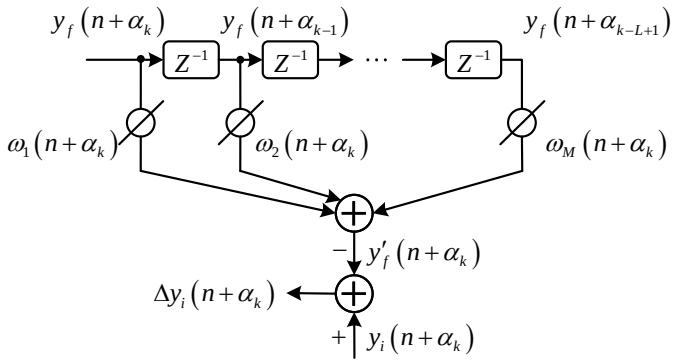


Figure 2. L-order self-interference reconstruction filter.

The residual signal after suppression is calculated by subtracting the reconstructed interference from the compressed received signal

$$\begin{aligned}\Delta y_i(n+\alpha_k) &= y_i(n+\alpha_k) - y'_f(n+\alpha_k)\\ &= y_i(n+\alpha_k) - \sum_{l=1}^{L}\omega_l(n+\alpha_k)\cdot y_f(n+\alpha_{k-l+1}).\end{aligned} \tag{20}$$

In vector form, the residual self-interference signal is given by

$$\Delta\mathbf{y}_i(n+\alpha_k) = [\Delta y_i(n+\alpha_1),\ldots,\Delta y_i(n+\alpha_k)]^T. \tag{21}$$

The final residual signal $\Delta\mathbf{y}$ consists of three components: the residual self-interference $\Delta\mathbf{y}_i$, the compressed SOI $\mathbf{y}_u$, and the compressed noise $\mathbf{v}_\varphi$

$$\begin{aligned}\Delta\mathbf{y} &= \mathbf{y} - \mathbf{y}'_f \\ &= \mathbf{y}_i + \mathbf{y}_u + \mathbf{v}_\varphi - \mathbf{y}'_f \\ &= \Delta\mathbf{y}_i + \mathbf{y}_u + \mathbf{v}_\varphi. \end{aligned} \tag{22}$$

3.3. SOI Reconstruction

After digital domain self-interference cancellation, the residual signal $\Delta\mathbf{y}$ is used for reconstructing the SOI, denoted as $\mathbf{r}_u$. As shown in Equation (22), the interference cancellation process does not alter the structure of the compressed SOI component $\mathbf{y}_u$, ensuring compatibility with standard reconstruction algorithms.

While the suppression procedure does not introduce structural distortion to the SOI, it does influence the effective signal-to-noise ratio (SNR). In the ideal case of perfect cancellation, the reconstruction quality of $\mathbf{r}_u$ is equivalent to that in an interference-free environment. However, in practical scenarios, non-ideal factors such as time or frequency synchronization errors may lead to residual self-interference $\Delta\mathbf{y}_i$ remaining in the signal. This residual acts as colored noise, thereby degrading the SNR and ultimately reducing the fidelity of the reconstructed SOI.

Accurate interference suppression is therefore crucial to maintaining reliable reconstruction performance under the compressed sensing framework.

The proposed architecture involves a trade-off between computational complexity and performance. By employing sub-Nyquist sampling through the NYFR, the ADC workload and data rate are reduced by a factor of N/M, which in turn lowers the computational complexity of the linear reconstruction filter from $\mathcal{O}(L \cdot N)$ to $\mathcal{O}(L \cdot M)$ per sample. This reduction comes at the cost of an additional compressed sensing reconstruction step to recover the SOI. The primary benefit, however, is substantially improved robustness to synchronization errors: for a given computational complexity, the compressed system can achieve higher suppression gain, or alternatively, relax the requirements on timing and frequency synchronization. Such a trade-off is particularly advantageous for IoT devices, where slight increases in digital processing complexity are acceptable in return for significantly enhanced interference suppression and a simpler RF front-end design.

This section analyzes the impact of fractional delay on the self-interference suppression performance. The fractional delay is modeled by an ideal fractional delay filter as follows

$$\begin{aligned} b(n - \Delta D) &= b(n) * \mathrm{sinc}(n - \Delta D) \\ &= A_{\Delta D} b(n) + b_{\Delta D}(n), \end{aligned} \tag{23}$$

where $A_{\Delta D} = \mathrm{sinc}(\Delta D)$ represents the attenuation coefficient caused by fractional delay. The term $b_{\Delta D}(n) = \sum_{\substack{i=-\infty \\ i\neq 0}}^{+\infty} b(n-i)\mathrm{sinc}(i - \Delta D)$ denotes the inter-symbol interference (ISI) component from adjacent symbols. The components $b_{\Delta D}(n)$ and $b(n)$ are uncorrelated.

The power of $b(n - \Delta D)$ and $b_{\Delta D}(n)$ can be expressed as [20]

$$\begin{aligned} P\{b(n - \Delta D)\} &= P\{b(n) * \mathrm{sinc}(n - \Delta D)\} \\ &= P\{b(n)\} \sum_{i=-\infty}^{\infty} \mathrm{sinc}^2(i - \Delta D) \\ &\approx P_b, \end{aligned} \tag{24}$$

$$P\{b_{\Delta D}(n)\} = P\{b(n)\} \sum_{\substack{i=-\infty \\ i\neq 0}}^{\infty} \mathrm{sinc}^2(i - \Delta D). \tag{25}$$

It should be noted that the fractional delay is implemented through a sinc-based filter, whose computational complexity mainly depends on the number of taps used in the approximation. A larger number of taps improves accuracy but also increases the number of multiplications per sample.

Assuming the wideband receiver can accurately estimate the self-interference channel gain $H_i A_{\Delta D}$, the reconstructed self-interference signal after compression is expressed as

$$\mathbf{y}'_f = H_i A_{\Delta D} \mathbf{y}_f = H_i A_{\Delta D} \boldsymbol{\varphi} \mathbf{r}_f, \tag{26}$$

where the residual self-interference component is denoted as

$$\Delta \mathbf{r}_i = H_i [b_{\Delta D}(n+1), \ldots, b_{\Delta D}(n+N)]^T. \tag{27}$$

Define the interference-to-noise ratio (INR) as

$$\gamma = \frac{H_i^2 P_b}{\sigma^2}, \tag{28}$$

where σ^2 denotes the noise power.

The self-interference suppression gain G without compression (i.e., without NYFR) is defined as

$$G = 10 \log_{10} \frac{P\{\mathbf{r}_i\} + \sigma^2}{P\{\Delta \mathbf{r}_i\} + \sigma^2}, \tag{29}$$

where $P\{\mathbf{r}_i\}$ and $P\{\Delta \mathbf{r}_i\}$ denote the power of the original self-interference and the residual self-interference signals, respectively.

Based on Equations (24) and (25), the powers can be approximated as

$$P\{\mathbf{r}_i\} = P\Big\{ H_i [b(n+1-\Delta D), \ldots, b(n+N-\Delta D)]^T \Big\} \approx H_i^2 P_b, \tag{30}$$

$$\begin{aligned} P\{\Delta \mathbf{r}_i\} &= P\Big\{ H_i [b_{\Delta D}(n+1), \ldots, b_{\Delta D}(n+N)]^T \Big\} \\ &= H_i^2 P_b \sum_{i=1}^{N} \mathrm{sinc}^2(i - \Delta D) + \sum_{i=-N}^{-1} \mathrm{sinc}^2(i - \Delta D). \end{aligned} \tag{31}$$

Substituting (28), (30), and (31) into (29), the suppression gain is

$$\begin{aligned} G &= 10 \log_{10} \left(\frac{H_i^2 P_b + \sigma^2}{H_i^2 P_b \left[\sum_{i=1}^{N} \mathrm{sinc}^2(i - \Delta D) + \sum_{i=-N}^{-1} \mathrm{sinc}^2(i - \Delta D) \right] + \sigma^2} \right) \\ &= 10 \log_{10} \left(\frac{\gamma + 1}{\gamma \left[\sum_{i=1}^{N} \mathrm{sinc}^2(i - \Delta D) + \sum_{i=-N}^{-1} \mathrm{sinc}^2(i - \Delta D) \right] + 1} \right). \end{aligned} \tag{32}$$

Similarly, the suppression gain after NYFR compression is defined as

$$G_{\boldsymbol{\varphi}} = 10 \log_{10} \frac{P\{\mathbf{y}_i\} + \sigma_{\boldsymbol{\varphi}}^2}{P\{\Delta \mathbf{y}_i\} + \sigma_{\boldsymbol{\varphi}}^2}, \tag{33}$$

where σ_{φ}^2 denotes noise power after compression, and $P\{\mathbf{y}_i\}$ and $P\{\Delta\mathbf{y}_i\}$ denote the power of the compressed self-interference and residual signals, respectively.

Based on Equations (24) and (25), these powers can be approximated as

$$P\{\mathbf{y}_i\} = \sum_{j\in\boldsymbol{\alpha}} P\{H_i b(n+j-\Delta D)\} \approx H_i^2 P_b, \tag{34}$$

$$\begin{aligned} P\{\Delta\mathbf{y}_i\} &= P\left\{H_i[b_{\Delta D}(n+\alpha_1),\ldots,b_{\Delta D}(n+\alpha_M)]^T\right\} \\ &\approx H_i^2 P_b\left[\sum_{i\in\boldsymbol{\alpha}} \mathrm{sinc}^2(i-\Delta D) + \sum_{i\in\boldsymbol{\alpha}-N} \mathrm{sinc}^2(i-\Delta D)\right]. \end{aligned} \tag{35}$$

Substituting (28), (34), and (35) into (33), the suppression gain after compression is

$$\begin{aligned} G_{\boldsymbol{\varphi}} &= 10\log_{10}\left(\frac{P\{\mathbf{y}_i\}+\sigma_{\boldsymbol{\varphi}}^2}{P\{\Delta\mathbf{y}_i\}+\sigma_{\boldsymbol{\varphi}}^2}\right) \\ &= 10\log_{10}\left(\frac{H_i^2P_b+\sigma_{\boldsymbol{\varphi}}^2}{H_i^2P_b\left[\sum_{i\in\boldsymbol{\alpha}}\mathrm{sinc}^2(i-\Delta D)+\sum_{i\in\boldsymbol{\alpha}-N}\mathrm{sinc}^2(i-\Delta D)\right]+\sigma_{\boldsymbol{\varphi}}^2}\right) \\ &= 10\log_{10}\left(\frac{\gamma+1}{\gamma\left[\sum_{i\in\boldsymbol{\alpha}}\mathrm{sinc}^2(i-\Delta D)+\sum_{i\in\boldsymbol{\alpha}-N}\mathrm{sinc}^2(i-\Delta D)\right]+1}\right). \end{aligned} \tag{36}$$

From Equations (32) and (36), the self-interference suppression performance depends on the INR, fractional delay, and ISI. As shown in Figure 3, the suppression performance degrades with increasing fractional delay. The NYFR compression reduces the effect of ISI, thus improving suppression compared to the uncompressed receiver under identical fractional delay.

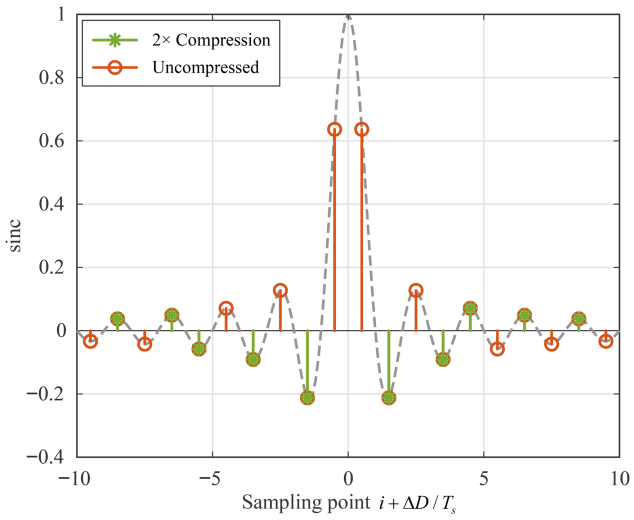


Figure 3. Illustration of ISI before and after compression.

4. Simulation

In this section, MATLAB 2022b simulations are performed to evaluate the digital domain self-interference suppression method and verify the impact of fractional delay on suppression performance in the CS-based wideband receiver. The simulation scenario assumes that the self-interference signal and the SOI operate at the same frequency, which makes it difficult for conventional receivers to extract valid information from the received signal.

The simulation parameters are summarized in Table 1. These parameters are chosen to reflect practical IoT scenarios: the carrier frequency of 2.4 GHz corresponds to widely used IoT bands (e.g., Wi-Fi, Bluetooth), the SOI bandwidth of 1 MHz represents narrowband IoT signals such as LoRa, the interference bandwidth of 5 MHz models wider-band coexisting devices, the fractional delay range (0∼0.5 T_s) captures typical multipath-induced delays, and the INR range (10∼60 dB) covers both weak and strong interference conditions. All simulations are conducted using the Monte Carlo method, with each point representing an average over 500 Monte Carlo trials to reduce statistical variation.

Table 1. Simulation parameters.

Parameter	Value
Original Sampling Rate	100 MHz
Compressed Sampling Rate	50 MHz
Carrier Frequency	2.4 GHz
Bandwidth of SOI	1 MHz
Interference Signal Bandwidth	5 MHz
Fractional Delay Range	0∼0.5 T_s
Interference-to-Noise Ratio	10∼60 dB

Figure 4 illustrates the variation in self-interference suppression gain with fractional delay under different INR levels. The simulation results closely match the theoretical analysis. When the INR is 10 dB or 20 dB, the impact of fractional delay on suppression gain is negligible, indicating that noise dominates suppression performance at low INR. However, as INR increases to 40 dB or 60 dB, the suppression gain degrades significantly with increasing fractional delay, eventually converging to about 29 dB. This shows that at high INR levels, suppression gain becomes highly sensitive to fractional delay.

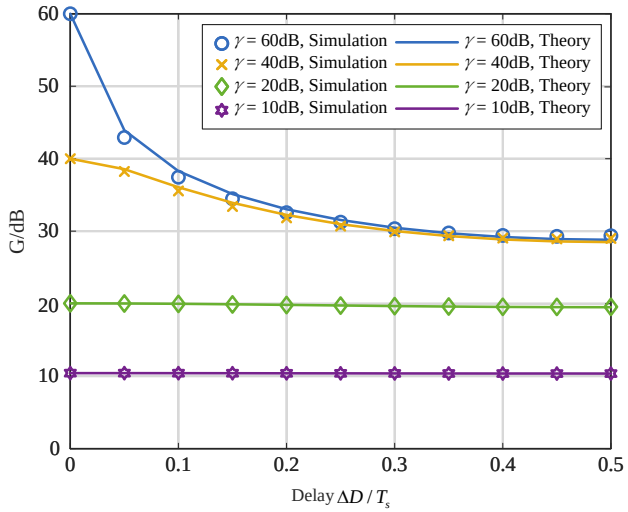


Figure 4. Relationship between fractional delay and self-interference suppression gain.

Figure 5 shows the variation in self-interference suppression gain with INR at various fractional delays. Simulation results agree well with theoretical predictions. When fractional delay $\Delta D = 0$, indicating ideal synchronization, suppression gain increases monotonically with INR. At an INR of 60 dB, suppression gain reaches approximately 60 dB, implying near-complete suppression of self-interference to the noise floor.

For fractional delays ranging from $0.05T_s$ to $0.3T_s$, suppression gain initially increases with INR but saturates beyond a certain point. Below 20 dB INR, suppression gains across different fractional delays converge, consistent with noise-dominated suppression. As

INR grows, differences in suppression gains for varying fractional delays become more pronounced. At 60 dB INR, suppression gains are approximately 43 dB, 38 dB, and 30.4 dB for increasing fractional delays, demonstrating that fractional delay limits suppression gain under high INR conditions.

Figure 6 depicts the impact of signal compression via the Nyquist Folding Receiver (NYFR) on suppression gain in the presence of fractional delay. The three groups of curves show a consistent trend of suppression gain degradation with increasing fractional delay under identical INR levels. At 10 dB INR, the effect of compression on suppression gain is minimal. However, when the INR is 30 dB and 60 dB, the uncompressed system exhibits the lowest suppression gain, while the system with 4× compression achieves the best performance. Moreover, as the fractional delay increases, the performance gap between the 2× compressed and uncompressed systems continues to widen, whereas the gap between the 4× and 2× compressed systems remains almost unchanged. Specifically, when the INR is 60 dB and the fractional delay is 0.5, the suppression gain of the 4× compressed system is 1 dB higher than that of the 2× compressed system, and 7.5 dB higher compared with the uncompressed case. These results clearly demonstrate that the NYFR-based compressive sensing receiver exhibits stronger robustness to fractional delay in the process of self-interference suppression.

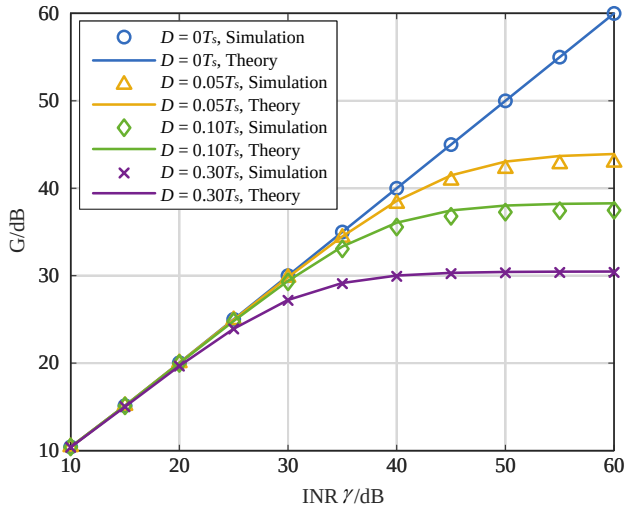


Figure 5. Relationship between INR and self-interference suppression gain under different fractional delays.

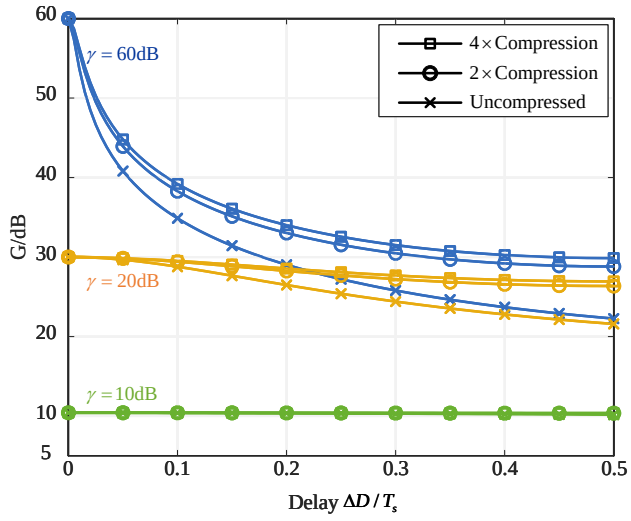


Figure 6. Effect of NYFR-based compression and fractional delay on self-interference suppression gain.

Figure 7 compares the self-interference suppression gain of receivers with and without NYFR compression under different fractional delays and INR values. When fractional delay is zero, suppression gain is limited by noise. For fractional delays of 0.1 and 0.3, suppression gain increases with INR and eventually saturates. In both scenarios, suppression gain with 2× compression consistently exceeds that without compression. For a fractional delay of 0.1 and INR above 40 dB, the gain difference stabilizes around 3 dB. When the delay is 0.3 and INR exceeds 35 dB, the difference stabilizes near 4.5 dB. These results indicate that under high INR, the effects of noise and NYFR compression on suppression gain remain stable.

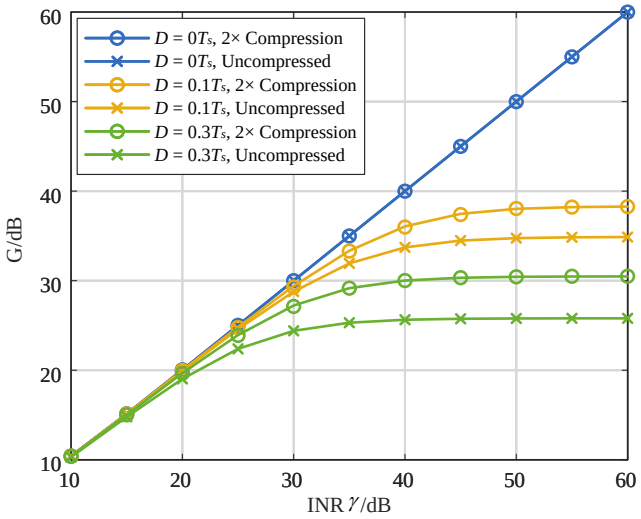


Figure 7. Comparison of self-interference suppression gain with and without NYFR compression under varying fractional delays and INR.

5. Conclusions

This paper presented a real-time-sensing-assisted intelligent communication architecture for IoT, which addresses the self-interference from the communication transmitter to the wideband sensing receiver. A digital domain self-interference suppression scheme based on the NYFR was developed for wideband compressed sensing systems under fractional delay. A closed-form expression was derived to quantify the impact of time synchronization errors on suppression performance. Simulation results validated the analysis and showed that NYFR compression improves suppression gain by up to 6.9 dB compared to uncompressed receivers under the same fractional delay. These results demonstrate that NYFR-based compression enhances robustness against fractional delay, making it a promising solution for real-time-sensing-assisted communication in dense IoT environments. The current work is limited to MATLAB simulations without hardware validation, and further study is needed on scalability to massive IoT scenarios and robustness under RF nonidealities. As future work, we will investigate adaptive filter design, hardware-in-the-loop testing, and machine learning-based extensions to enhance both robustness and computational efficiency.

Author Contributions: Conceptualization, S.Z. and L.Q.; methodology, L.Q.; software, S.Z.; validation, S.Z., L.Q. and W.S.; formal analysis, S.Z. and W.S.; investigation, L.Q.; resources, L.Q.; data curation, S.Z.; writing—original draft preparation, L.Q.; writing—review and editing, S.Z. and W.S.; visualization, S.Z.; supervision, L.Q.; project administration, L.Q. All authors have read and agreed to the published version of the manuscript.

Funding: This research received no external funding.

Data Availability Statement: The original contributions presented in this study are included in the article. Further inquiries can be directed to the corresponding author.

Conflicts of Interest: The author Shengfeng Zhang was employed by the 8th Research Academy of China State Shipbuilding Corporation. The remaining authors declare that the research was conducted in the absence of any commercial or financial relationships that could be construed as a potential conflict of interest.

Abbreviations

The following abbreviations are used in this manuscript:

CS	Compressive sensing
NYFR	Nyquist folding receiver
ADC	Analog-to-digital converter
DAC	Digital-to-analog converter
RF	Radio frequency
ISI	Inter-symbol interference
INR	Interference-to-noise ratio
SNR	Signal-to-noise ratio
SOI	Signal of interest

References

1. Garg, H.; Dave, M. Securing IoT Devices and SecurelyConnecting the Dots Using REST API and Middleware. In Proceedings of the 2019 4th International Conference on Internet of Things: Smart Innovation and Usages (IoT-SIU), Ghaziabad, India, 18–19 April 2019; pp. 1–6.
2. Ramsudhan, G.; Hrudaya, G.; Krishnan, R. Blockchain Enabled IoT Security for Smart Home Network. In Proceedings of the 2025 13th International Conference on Smart Grid (icSmartGrid), Glasgow, UK, 27–29 May 2025; pp. 1–6.
3. Zhou, Z.; Li, X.; He, J.; Bi, X.; Chen, Y.; Wang, G.; Zhu, P. 6G Integrated Sensing and Communication—Sensing Assisted Environmental Reconstruction and Communication. In Proceedings of the ICASSP 2023—2023 IEEE International Conference on Acoustics, Speech and Signal Processing (ICASSP), Rhodes Island, Greece, 4–10 June 2023; pp. 1–5.
4. Jiang, K.; Tian, K.; Feng, H.; Zhao, Y.; Wang, D.; Gao, J.; Cao, S.; Zhang, X.; Li, Y.; Yuan, J.; et al. Distributed UAV Swarm Augmented Wideband Spectrum Sensing Using Nyquist Folding Receiver. *IEEE Trans. Wirel. Commun.* **2024**, *23*, 14171–14184. [CrossRef]
5. Jin, Y.; Zhang, M.; Gao, Y.; Liu, S. Efficient Millimeter-Wave Beam Prediction: A Wi-Fi Sensing-Assisted Deep Learning Approach. *IEEE Sens. J.* **2024**, *24*, 42210–42218. [CrossRef]
6. Maleh, R.; Fudge, G.L.; Boyle, F.A.; Pace, P.E. Analog-to-information and the Nyquist folding receiver. *IEEE J. Emerg. Sel. Top. Circuits Syst.* **2012**, *2*, 564–578. [CrossRef]
7. Sui, J.; Liu, Z.; Wei, X.; Li, X.; Peng, B.; Liao, D. Velocity false target identification in random pulse initial phase radar based on compressed sensing. In Proceedings of the 2015 3rd International Workshop on Compressed Sensing Theory and Its Applications to Radar, Sonar and Remote Sensing (CoSeRa), Pisa, Italy, 17–19 June 2015; pp. 179–183.
8. Tang, J.; Qiu, Z.; Cao, B.; Yuan, Z. Parameter Estimation of Multiple Linear Frequency Modulation Signals Sensed by Nyquist Folding Receiver Using Periodic Linear Frequency Modulation Local Oscillator. *IEEE Sens. J.* **2025**, *25*, 31120–31134. [CrossRef]
9. Qiu, Z.; Wang, P.; Zhu, J.; Tang, B. Estimation of both Nyquist zone index and code rate for BPSK radar signal intercepted by Nyquist folding receiver. *IET Radar Sonar Navig.* **2017**, *11*, 1652–1663. [CrossRef]
10. Akama, C.; Nunoo, S.; Lee, K.J.; Annan, J.K. Optimal Beamforming for Full-Duplex Integrated Sensing, Communication and Computation Systems. *IEEE Access* **2025**, *13*, 152335–152345. [CrossRef]
11. Liu, G.; Yu, F.R.; Ji, H.; Leung, V.C.; Li, X. In-band full-duplex relaying: A survey, research issues and challenges. *IEEE Commun. Surv. Tutor.* **2015**, *17*, 500–524. [CrossRef]
12. Deo, P.; Mirshekar-Syahkal, D.; Zheng, G.; Pal, A.; Mehta, A. Broadband antenna for passive self-interference suppression in full-duplex communications. In Proceedings of the IEEE Radio and Wireless Symposium, Anaheim, CA, USA, 15–18 January 2018; pp. 243–245.
13. Ju, H.; Xu, Y.; He, D.; Yang, N.; Li, H.; Zhang, W.; Wu, Y. An RF Self-Interference Cancellation method for In-Band Distribution Link in ATSC 3.0. In Proceedings of the 2024 IEEE International Symposium on Broadband Multimedia Systems and Broadcasting (BMSB), Toronto, ON, Canada, 19–21 June 2024; pp. 1–5.

14. Liu, Y.; Quan, X.; Pan, W.; Tang, Y. Digitally assisted analog interference cancellation for in-band full-duplex radios. *IEEE Commun. Lett.* **2017**, *21*, 1079–1082. [CrossRef]
15. Jiang, Y.; Xu, C.; Ding, W.; Zhao, N.; Liu, C. Nonlinear characteristic and its suppression for cosite interference cancellation system. In Proceedings of the 2017 7th IEEE International Conference on Electronics Information and Emergency Communication (ICEIEC), Macau, China, 21–23 July 2017; pp. 591–594.
16. Guo, W.; Song, C.; Xia, X.; Hu, F.; Zhao, H.; Shao, S.; Tang, Y. Analysis of cooperative jamming cancellation with imperfect time synchronization in physical layer security. *IEEE Wirel. Commun. Lett.* **2020**, *10*, 335–338. [CrossRef]
17. Guo, W.; Hu, H.; He, Y.; Yan, M.; Zhao, H.; Shao, S. Impacts of Clock Jitter on Cooperative Jamming Cancellation. In Proceedings of the IEEE Global Communications Conference, Rio de Janeiro, Brazil, 4–8 December 2022; pp. 4142–4147.
18. Jing, W.; Tang, J.; Cao, S.; Liu, P. Time synchronization with delay estimation and joint clock skew and offset estimation for UAV networks. In Proceedings of the International Conference on Communication Technology, Wuxi, China, 20–22 October 2023; pp. 1662–1667.
19. Donoho, D.L. Compressed sensing. *IEEE Trans. Inf. Theory* **2006**, *52*, 1289–1306. [CrossRef]
20. He, Y.; Zhao, H.; Guo, W.; Shao, S.; Tang, Y. A Time-Robust Digital Self-Interference Cancellation in Full-Duplex Radios: Receiver Design and Performance Analysis. *IEEE Access* **2020**, *8*, 185021–185031. [CrossRef]

Disclaimer/Publisher's Note: The statements, opinions and data contained in all publications are solely those of the individual author(s) and contributor(s) and not of MDPI and/or the editor(s). MDPI and/or the editor(s) disclaim responsibility for any injury to people or property resulting from any ideas, methods, instructions or products referred to in the content.